Exploration Geophysics (2004) 35, 56–61
Butsuri-Tansa (Vol. 57, No. 1)
Mulli-Tamsa (Vol. 7, No. 1)

Permeability imaging in granitic rocks based on surface resistivity profiling

Hiroshi Sudo[1] Toshikazu Tanaka[1] Tsuyoshi Kobayashi[2] Tatsutoshi Kondo[3] Toru Takahashi[4] Masaharu Miyamoto[5] Mitsuru Amagai[5]

Key Words: permeability, resistivity, granitic rock

ABSTRACT

In order to image the distribution of permeability in granitic rocks, we carried out two-dimensional (2D) resistivity profiling, together with in-situ permeability tests, electrical logging of boreholes, and resistivity measurements of rock core samples in a laboratory. Based on the electrical logging and in-situ permeability data from boreholes, we obtained empirical equations which relate resistivity and permeability of the granitic rocks in the area studied. We then applied the empirical equation to a 2D resistivity section, to produce a 2D permeability section of the granitic rocks. In this paper, we present details of the field data and of the procedure for conversion from the resistivity section to a permeability section. The observed relationship between resistivity and permeability of the rocks is also discussed.

INTRODUCTION

Geophysical methods that can delineate subsurface geophysical parameters, such as resistivity and seismic velocity, have been improved significantly thanks to advanced field equipment and reliable interpretation techniques developed in the past decade. They can provide more accurate and higher-resolution subsurface geophysical images than before. However, in civil engineering applications, geotechnical or engineering parameters such as mechanical strength or permeability of rocks are required, rather than geophysical parameters.

In recent tunnel construction projects, there has been an increasing requirement for hydrogeological parameters such as the permeability of rocks, as well as the mechanical parameters, for environmental assessment and countermeasure planning, as well as for safe and economical construction. Conventionally, the hydrogeological model of a tunnel route has been constructed by interpolating and extrapolating the permeability data obtained from in-situ testing in a few boreholes along the route, in combination with geological information. Geophysical methods can provide two-dimensional (2D) images of geophysical parameters such as resistivity along a tunnel route. Such images could be a very powerful tool if a practical technique to transform geophysical parameters to geotechnical ones could be established.

We have therefore attempted to image the permeability distribution along a planned tunnel route, using a subsurface resistivity section together with in-situ measurements of the relevant parameters. Many researchers have studied the relationship between resistivity and permeability of rocks, using rock core samples and geophysical logging data. Katsube and Hume (1987), Nishimaki et al. (1999), and Suzuki (2002) have shown that rock permeability is proportional to some power of the rock resistivity. Matsui et al. (1997) have shown that resistivity increases with increasing permeability at low to moderate values of resistivity, while resistivity increases with decreasing permeability where the range of resistivity is moderate to high, in granitic rocks. Tamai et al. (2001) have presented results showing 2D permeability zoning from the relationship between water content by volume and permeability of rocks, in Paleozoic rocks. Ogata et al. (1992) found that the rock resistivity of Tertiary sandstones, mudstones, and conglomerates is directly proportional to permeability. On the other hand, Tanaka et al. (2002) have shown that resistivity increases as permeability decreases for fresh granite with some fractures.

In this paper, we show a field example of the relationship between resistivity and permeability and discuss a rock model that can explain it. We then transform a 2D resistivity section to a 2D permeability section for actual field data and so demonstrate that the geophysical method can be very useful in obtaining a regional distribution of geotechnical parameters.

GEOLOGY OF THE INVESTIGATION AREA

Our investigation area is located at a northern scarp of Mt. Tsukuba in Ibaraki Prefecture, central Japan, where geological, geophysical and geotechnical investigations were carried out as a preliminary investigation for a tunnel construction. Figures 1 and 2 show a surface geological map, and a geological section along the tunnel route, respectively. The whole area is underlain by homogeneous and fine-grained granite of late Cretaceous to early Palaeogene age, partly penetrated by small pegmatite dykes. A fault F-1, which runs across the tunnel route, was found at outcrop A (Figure 1). The fault strikes N49°W and dips 80°N.

The granitic rocks in this survey area have dominant joint systems oriented in NW–SE and NE–SW directions, identified by aerial photograph interpretation. The jointing in the NW–SE direction is especially distinct.

[1] *Tokyo Branch Office, OYO Corporation*
3-2-1 Ohtsuka, Bunkyo-ku,
Tokyo, Japan 112-0012
Phone: +81-3-3946-3111
Facsimile: +81-3-3946-3118
E-mail: sudou-hiroshi@oyonet.oyo.co.jp

[2] *Technical Centre, OYO Corporation*
2-61-5 Toro-chyo, Minuma-ku, Saitama-shi
Saitama, Japan 331-8688

[3] *Geo Holon Partners*
537-4 Nakagawa, Minuma-ku, Saitama-shi
Saitama, Japan 337-0043

[4] *Tsukuba Technical Development Centre, OYO Corporation*
43 Miyukigaoka, Tsukuba-shi
Ibaraki, Japan 305-0841

[5] *Ibaraki Prefectural Government*
978-6 Kasahara-cho, Mito-shi,
Ibaraki, Japan 310-8555

Manuscript received July 28, 2003; accepted October 6, 2003. Part of this paper was presented at the 6th SEGJ International Symposium (2003).

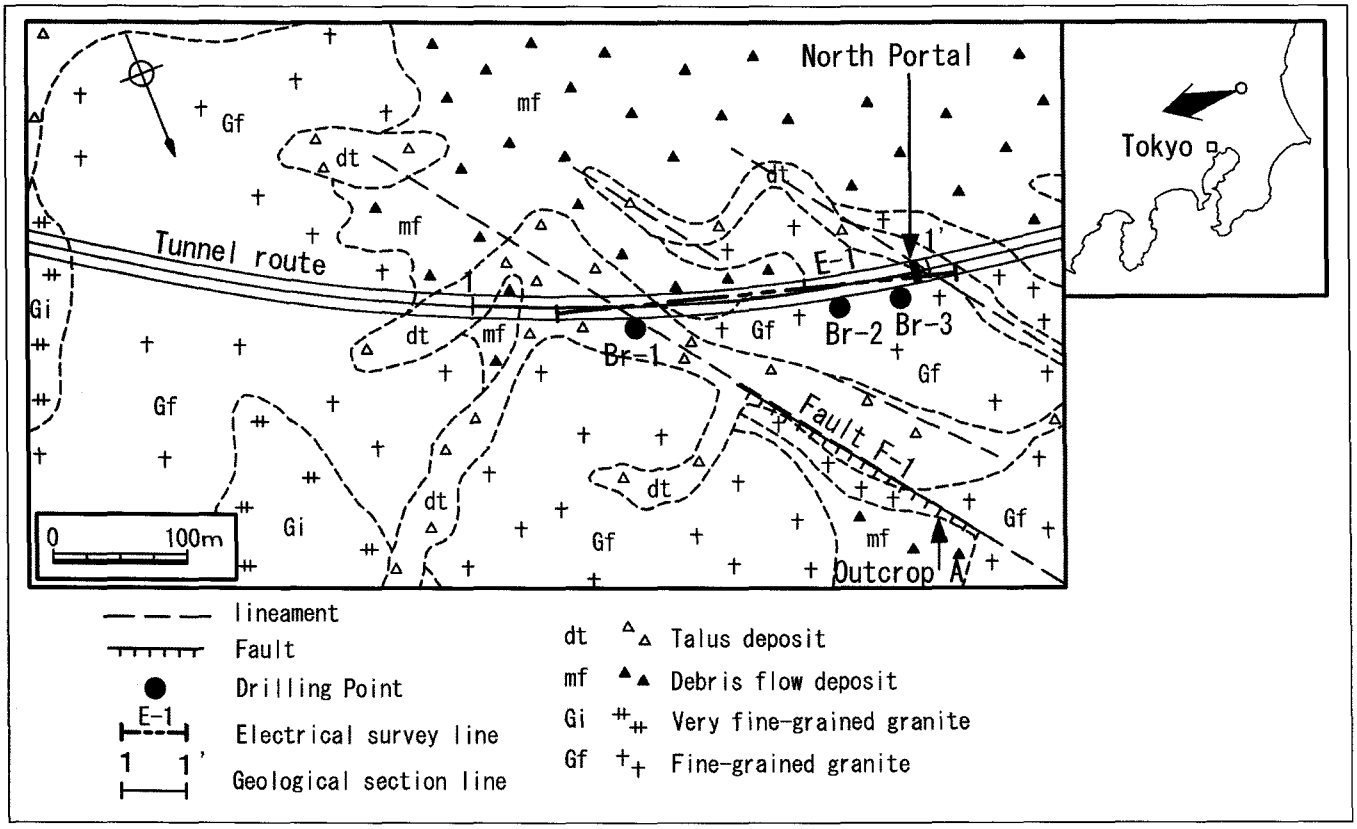

Fig. 1. Surface geological map of the investigation area.

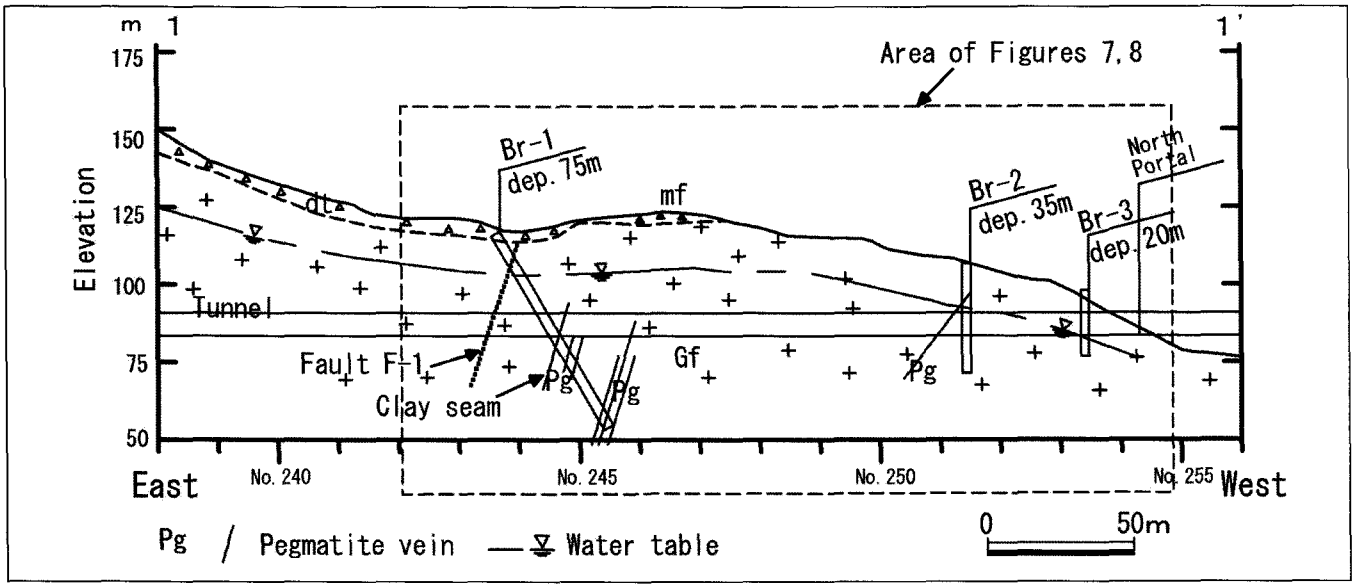

Fig. 2. Geological cross section near the north portal, along the line 1-1' shown in Figure 1.

MEASUREMENTS OF RESISTIVITY AND PERMEABILITY

To obtain a resistivity section of the investigation area, surface resistivity measurements were performed. In addition, electrical logging and in-situ permeability tests were conducted in three boreholes drilled along the tunnel route. In addition, the resistivity of rock core samples from the boreholes was measured in a laboratory. The details of each measurement are described in the following subsections.

Surface resistivity profiling

A resistivity section was obtained along Line E-1, which was 300 m long, along the tunnel route (Figure 1). The pole-pole array was used, with a smallest electrode interval of 5 m and maximum interval of 75 m. Finite element forward modelling and a non-linear inversion method (Shima et al., 1995) were applied to obtain a 2D resistivity section. The resultant resistivity section is shown in Figure 7, for comparison with the permeability section.

Normal-array resistivity logging

Normal-array resistivity logging was carried out in the three boreholes (Br-1, Br-2, and Br-3). The logging tool has ten electrodes with an interval of 0.2 m to measure electrical potential data for various electrode spacings, from 0.2 m to 2.0 m. A true formation resistivity around the boreholes is evaluated by using the apparent resistivity data from the ten different spacings (Imamura, 1993).

In-situ permeability measurements

The permeability of rocks was measured in the boreholes by the low-pressure Lugeon test (Japan Institute of Construction Engineering, 1984), and the Johnstone's Formation Tester (JFT) method. The former test estimates permeability by measuring a water injection rate in a borehole and the latter measures a piezometric hydraulic pressure at the level of the planned tunnel route. The measurements were carried out at several depths, representing each weathering grade of the rocks in the three boreholes. The length of the measurement interval was 3 m, in principle. The permeability was calculated by the following equation (Bureau of Reclamation, 1974):

$$k = \frac{Q \ln\left(\frac{L}{r}\right)}{2\pi HL}, \qquad (1)$$

where k is permeability (more correctly hydraulic conductivity), Q is flow quantity, H is water head difference, L is the length of the measurement interval, and r is the radius of the borehole. The values of Q and H are measured by the low-pressure Lugeon test.

Figure 3 shows the resistivity logging data, in-situ permeability data, photographs of rock core samples, and crack characteristics in the three boreholes. Figure 3(a) shows data from borehole Br-1, in which closed cracks, open cracks, and clay-filled cracks are observed. Open cracks are dominant in this borehole. Data number 10 includes cracks filled with white clay and this interval shows the lowest resistivity. Figure 3(b) shows the data from weathered rocks in boreholes Br-2 and Br-3, in which the cracks are filled with sand, or a clay and sand mixture.

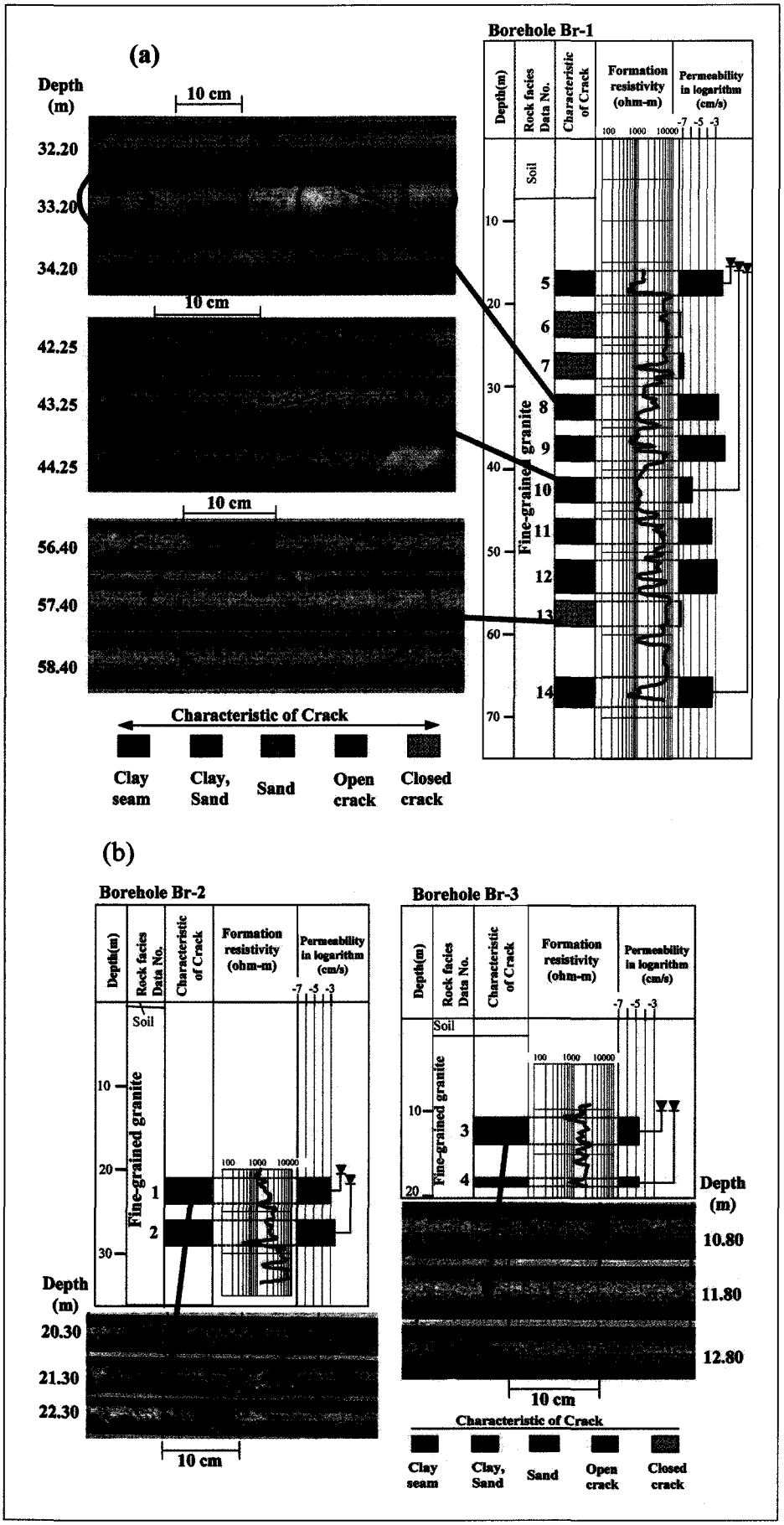

Fig. 3. Photographs of rock core samples and borehole data including resistivity logs, in-situ permeability, and crack characteristics in (a) borehole Br-1 and (b) boreholes Br-2 and Br-3.

Core No.	Borehole	Depth (m)	Weathering grade
1	Br–1	16.05–16.10	B
2	Br–1	32.05–32.10	B
3	Br–1	56.05–56.10	B
4	Br–1	65.05–65.10	B
5	Br–1	7.53–7.58	C
6	Br–2	33.10–33.30	C
7	Br–3	15.00–15.20	C

Table 1. Rock core samples used for the laboratory resistivity measurement.

Resistivity measurements of rock core samples

Generally, the resistivity of rocks varies with many factors such as mineral composition, porosity, fracture aperture, resistivity of fracture-filling fluids, and fluid saturation. In order to investigate the influence of fluid saturation on the resistivity, we measured the resistivity of rock core samples with various degrees of fluid saturation in a vacuum container. The fluid used in the vacuum container was groundwater obtained from borehole Br-2. The resistivity of this groundwater was 82 Ω.m. Seven rock core samples from the three boreholes were used for the experiment (Table 1). The rock core samples were divided into two groups based on the grade of weathering: B for fresh rocks and C for weathered. Four ring electrodes, two current electrodes and two potential electrodes, were used to measure the resistivity of the samples. Resistivity was calculated as:

$$R = \frac{S}{L} \cdot \frac{V}{T}, \qquad (2)$$

where R is resistivity, V is potential difference between two electrodes, I is electrical current injected, S is the cross sectional area, and L is the length of the sample.

Figure 4 shows the relationship between water saturation and resistivity of the rock core samples measured. This figure reveals that the measured resistivity is clearly divided into two groups by the weathering grade (B or C). Resistivity of the rocks depends on both fluid saturation and weathering grade. These observations indicate that it would be very difficult to use the resistivity values of partially saturated rocks for the evaluation of permeability. Therefore, in this study, we have focused only on the resistivity data of saturated rocks, which means those rocks below the groundwater table.

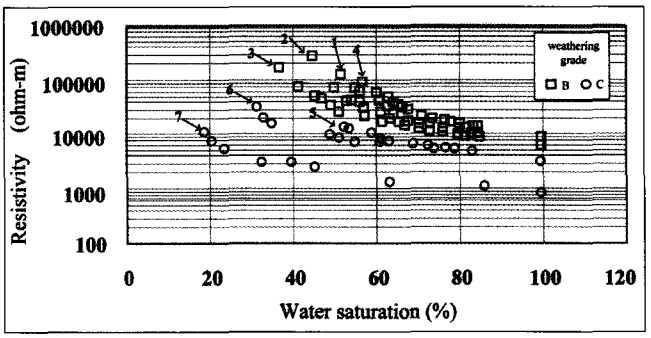

Fig. 4. Relationship between resistivity and water saturation of rock core samples shown in Table 1 with respect to weathering grade.

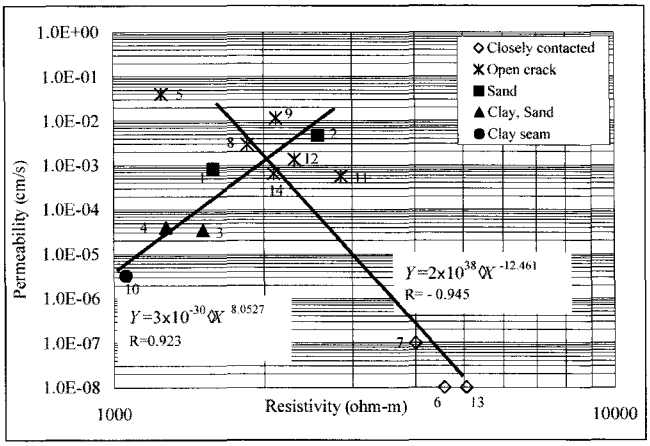

Fig. 5. Relationship between resistivity and permeability measured in the three boreholes shown in Table 2.

DISCUSSION

Relationship between permeability and resistivity in the boreholes

Representative resistivity values were evaluated by averaging the resistivity values of the electric logs over the interval of the in-situ permeability tests. The resistivity values thus obtained for each interval in the three boreholes are shown in Table 2, together with the in-situ permeability data. In this table, the characteristics of cracks observed at each interval and the weathering grade of rocks are also shown. Figure 5 graphs the relationship between resistivity and permeability shown in Table 2.

Data No.	Borehole	Measurement depth (m)	Resistivity (ohm-m)	Permeability (cm/s)	Characteristics of crack	Weathering grade
1	Br–2	20.6–24.0	1582	8.25E–04	Sand	C
2	Br–2	26.0–29.0	2561	4.68E–03	Sand	C
3	Br–3	11.0–14.0	1511	3.44E–05	Clay, sand	C
4	Br–3	18.0–19.0	1275	3.94E–05	Clay, sand	C
5	Br–1	16.0–19.0	1250	3.99E–02	Open crack	B
6	Br–1	21.0–24.0	4575	1.00E–08	Closed crack	B
7	Br–1	26.0–29.0	4000	1.00E–07	Closed crack	B
8	Br–1	31.0–34.0	1850	2.94E–03	Open crack	B
9	Br–1	36.0–39.0	2110	1.15E–02	Open crack	B
10	Br–1	41.0–44.0	1061	3.22E–06	Clay seam	C
11	Br–1	46.0–49.0	2850	5.71E–04	Open crack	B
12	Br–1	51.0–55.0	2300	1.35E–03	Open crack	B
13	Br–1	56.0–60.0	5060	1.00E–08	Closed crack	B
14	Br–1	65.0–70.0	2090	6.47E–04	Open crack	B

Table 2. Resistivity and permeability measured in the three boreholes. Crack characteristics and weathering grades are also shown.

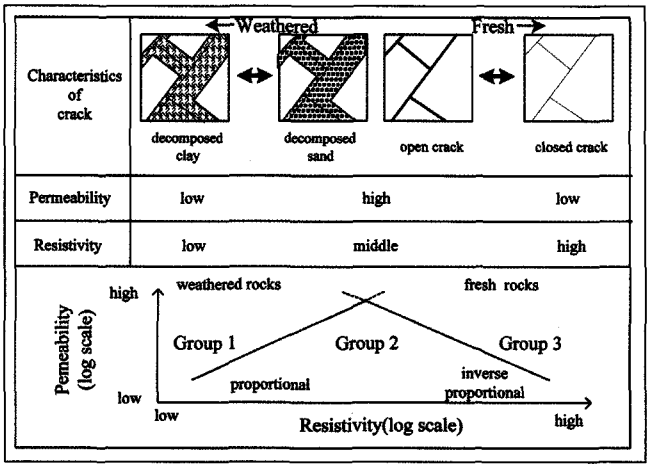

Fig. 6. Schematic diagram of a rock model that can explain the relationship between resistivity and permeability observed in this investigation.

The following observations are noted from Figure 5:

a) The data plotted in the figure are divided into three groups: Group 1 with the lowest resistivity and low permeability (data numbers 3, 4, and 10); Group 2 with moderate resistivity and high permeability (data numbers 1, 2, 5, 8, 9, 11, 12, and 14); and Group 3 with the highest resistivity and the lowest permeability (data numbers 6, 7, and 13).
b) The data of Group 1 are sampled from rocks with cracks filled with clay and from highly weathered rocks. The cracks have approximately 2-mm-thick fillings.
c) The data of Group 2 come from rocks with many cracks filled with sand or with a few cracks with no filling.
d) The data of Group 3 correspond to fresh and intact rocks with a few almost-closed cracks.

These relationships between resistivity and permeability of granitic rocks can be interpreted with crack models schematically illustrated in Figure 6. A fresh rock without cracks has high resistivity and low permeability. A rock with unfilled cracks has very high permeability, but relatively low resistivity, because pore water is electrically conductive and flows easily in open cracks. A rock with clay-filled cracks has low resistivity and low permeability because the clay has low resistivity but prevents pore water from flowing through the cracks.

Ogata et al. (1992) presented evidence that the permeability of sandstones, mudstones, and conglomerates of Miocene age is proportional to the apparent resistivity obtained from electric logs. They obtained the following empirical equations between the parameters:

$$Y = 3.545 \cdot 10^{-11} \cdot X^{3.9072} \quad (3)$$

for sandstones and mudstones and

$$Y = 1.295 \cdot 10^{-12} \cdot X^{4.2279} \quad (4)$$

for conglomerates, where Y is permeability in cm/s and X is apparent resistivity in Ω.m. On the other hand, Katsube and Hume (1987) showed inversely proportional relationships between permeability and the formation factor of core samples of granite,

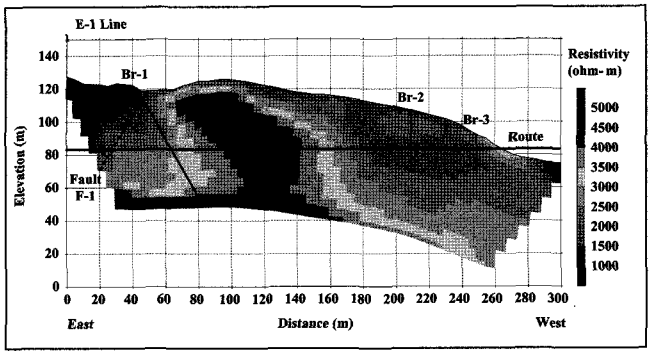

Fig. 7. 2D subsurface resistivity section of the line E-1 along the tunnel route.

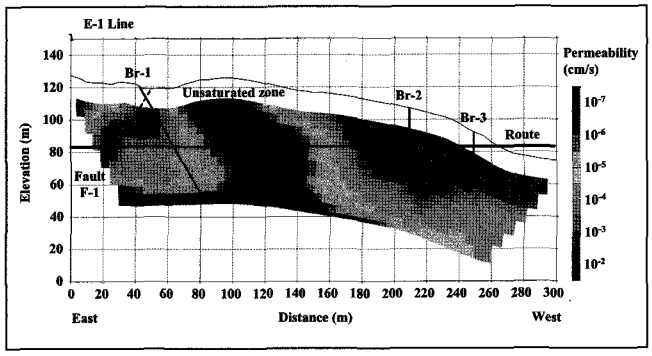

Fig. 8. 2D permeability section transformed from the resistivity section shown in Figure 7.

in a laboratory experiment. Both of these features are observed in our data, which suggests that the crack model proposed here is to some extent compatible with their interpretations.

Transformation from the resistivity section to the permeability section

As shown in Figure 5, permeability can be represented as a function of resistivity by a convex curve, whose peak corresponds to a resistivity of approximately 2000 Ω.m for these specific rocks. By fitting a straight line to each subgroup of data in log-log space, we can represent this relationship with the following two equations:

$$Y = 3 \cdot 10^{-30} \cdot X^{8.1} \quad (5)$$

for the resistivity below 2000 Ω.m, and

$$Y = 2 \cdot 10^{38} \cdot X^{-12.5} \quad (6)$$

for the resistivity above 2000 Ω.m, where X is resistivity and Y is permeability.

Using these two equations, we transformed the 2D subsurface resistivity section for Line E-1 (Figure 7) to a permeability section (Figure 8). As shown in Figure 4, resistivity is strongly influenced by the degree of water saturation. The groundwater table was estimated to be around 10 m in depth beneath the survey line, and

the near-surface zone shallower than this level was unsaturated. The above equations were derived for saturated rocks. Therefore, the transformation was applied only to the saturated zone below the groundwater table.

The estimated permeability values in Figure 8 range from 10^{-2} cm/s for weathered rocks to 10^{-7} cm/s for fresh and intact rocks. The permeability around the fault is found to be higher than elsewhere on the line. The permeability section thus obtained has not been validated yet, but will be evaluated at the excavation stage of the tunnel.

CONCLUSIONS

We transformed a 2D resistivity section to a permeability section for a further hydrogeological study along the planned tunnel route. For the transformation, we obtained a relationship between both parameters by analysing resistivity logs and in-situ permeability measurements in conjunction with crack characteristics observed from drilling cores. It was revealed that the relationship thus obtained could be interpreted as a schematic crack model with fillings of water, sand, clay, etc. This model was supported by the previously published research works.

The transformation presented here was made based on a site-specific cross-plot of the resistivity and permeability of granitic rocks. To generalize the method, other rock models should be constructed by studying the mutual relationship of many parameters and factors affecting permeability and resistivity of rocks. For this purpose, more case studies and data sets are required, and intensive rock physical studies should be performed in the future.

ACKNOWLEDGEMENTS

We are grateful to Ibaraki Prefectural Government for allowing us to use the data in this paper. We thank reviewers for their careful reading and constructive comments which have improved this paper.

REFERENCES

Bureau of Reclamation, 1974, *Earth manual, 2nd Ed.*

Imamura S., 1993, Array normal resistivity logging and its processing technique - Synthetic Focused Resistivity logging (SFR) and Borehole Resistivity Profiler (BRP): *Proceedings of the 89th SEGJ Conference*, 183–187.

Japan Institute of Construction Engineering, 1984, *Technical guide of Lugeon test*: Ministry of Construction, River Development Bureau, 5–19.

Katsube, T.J., and Hume, J.P., 1987, Permeability determination in crystalline rocks by standard geophysical logs: *Geophysics*, **52**, 342–352.

Matsui, T., Kamiide, S., and Park, S., 1977, An applicability of resistivity-based high-density prospecting to ground survey of mountain tunnel: *Tsuchi-to-kiso*, **45**, 20–22.

Nishimaki, H., Sekine, I., Saito, A., and Yoshinaka, R., 1999, Electrical resistivity of a rock and its correlation to engineering properties: *Butsuri-tansa*, **52**, 161–171.

Ogata, N., Ohsawa, H., Nakano, K., Yanagizawa, K., and Nishigaki, M., 1992, Relationship among lithology, permeability and resistivity and their application to modelling of hydrogeology: *J. Japan Soc. Eng. Geology*, **32**, 51–61.

Shima, H., Kajima, K., and Kamiya, H., 1995, *Resistivity image profiling*: Kokon Syoin.

Suzuki, K., 2002, Imaging techniques of geophysical properties for engineering by geophysical exploration: *J. Japan Soc. Eng. Geology*, **42**(6), 342–349.

Tamai, S., Irie, A., and Obata, D., 2001, Method for evaluating geophysical properties of rock mass with numerical modeling of groundwater flow: *Proceedings of the 31st Symposium on Rock Mechanics*, 336–340.

Tanaka, T., Sudo, H., Kobayashi, T., Kondo, T., Miyamoto, M., and Amagai, M., 2002, Conversion of a surface resistivity profile into permeability distribution: Proceedings, Symposium of Japan Soc. Eng. Geology, 251–254.